


 Cite this: *Nanoscale*, 2025, **17**, 4400

# Fluoride binding-modulated supramolecular chirality of urea-containing triarylamine and its photo-manifestation†

 Sijia Ma,<sup>a,b,c</sup> Xin Wen,<sup>a,b</sup> Yuqian Jiang,<sup>id</sup> <sup>c</sup> Jian Jiang,<sup>id</sup> \*<sup>c</sup> Wenchao Hao,<sup>a,b</sup> Li Zhang<sup>id</sup> \*<sup>a,b</sup> and Minghua Liu<sup>id</sup> \*<sup>a,b</sup>

In recent years, the regulation of anion-mediated chiral assemblies has gained significant interest. This study investigated the modulation of supramolecular chiroptical signals and chiral assembled structures in a triarylamine system containing a urea moiety through fluoride ion–urea bond interactions, aiming to understand the chiral sense amplification in supramolecular assemblies. Chiral triarylamine derivatives containing urea or amide units were synthesized and the self-assemblies were examined in the absence and presence of fluoride ions. The results revealed that the addition of F<sup>−</sup> led to an increase in the circular dichroism (CD) intensity for the triarylamine compounds containing urea, accompanied by a transformation of the nanofiber structure into chiral twists. Comparative studies with other anions confirmed the selective specificity for F<sup>−</sup>. Additionally, the combination of photo-induced triarylamine anion radicals allowed the F<sup>−</sup> in the system to be visualized through photoirradiation, resulting in distinct colour changes that were detectable by the naked eye. The research demonstrates that F<sup>−</sup> can selectively amplify supramolecular chirality through urea–F<sup>−</sup> interactions, which may have promising applications in the fields of sensing and chiroptical devices.

 Received 10th October 2024,  
Accepted 23rd December 2024  
DOI: 10.1039/d4nr04175e

[rsc.li/nanoscale](https://rsc.li/nanoscale)

## Introduction

Chiral assembly is the process in which molecular building blocks self-assemble into ordered, organized structures that express pronounced chiroptical signals or macroscopic chiral morphologies, such as twists, helical tubes, and toroids, through various non-covalent interactions.<sup>1–6</sup> The study of chiral supramolecular assemblies is crucial due to their potential in designing sophisticated materials<sup>7–10</sup> and offering a platform for exploring the significance of chirality in biological systems.<sup>11–13</sup> Owing to the nature of the non-covalent interactions that form self-assemblies, supramolecular chirality often exhibits smart response to external stimuli, such as pH,<sup>14</sup> solvents,<sup>15–17</sup> photoirradiation<sup>18–23</sup> and ion manipulation.<sup>24,25</sup> Anions,<sup>26–28</sup> being omnipresent in nature, play a crucial role in various chemical

and biological processes.<sup>29,30</sup> The utilization of anions to regulate assembly not only offers a new dimension to influence assembly processes,<sup>31,32</sup> but may also find diverse applications in the field of regulation of anion concentrations in living systems and the detection of anionic pollutants from agricultural, industrial, or military sources.<sup>33</sup> The fluoride anion,<sup>34</sup> as the smallest anion with high charge density and significant basicity, is particularly significant in the biological and medical fields.<sup>35</sup> Fluoride's contribution to dental health is well-recognized.<sup>36</sup> However, overexposure can result in serious health complications, including kidney failure and skeletal abnormalities.<sup>37</sup> Additionally, the detection of fluoride anions *via* supramolecular receptors is crucial for the identification of chemical warfare agents like Sarin,<sup>38</sup> which release fluoride during hydrolysis.<sup>39</sup> Consequently, fluoride anion-mediated supramolecular assembly has emerged as a topic of intense interest within the field of supramolecular chemistry.<sup>40,41</sup> So far, the fluoride anion-mediated regulation of chiral assemblies is relatively rarely documented,<sup>42</sup> whilst the utilization of amides,<sup>43</sup> ureas,<sup>44,45</sup> and thiourea as anion receptors in fluoride ion-regulated supramolecular systems has been extensively studied.

Herein, chiral triarylamine derivatives containing urea or amide units were utilized to interact with fluoride ions (F<sup>−</sup>). These compounds were designed to recognize F<sup>−</sup> mainly based on two considerations: firstly, the urea or amide moieties are introduced based on the hydrogen bonding interaction between

<sup>a</sup>Beijing National Laboratory for Molecular Science, CAS Key Laboratory of Colloid, Interface and Chemical Thermodynamics, Institute of Chemistry, Chinese Academy of Sciences, No. 2 ZhongGuanCun BeiYiJie, 100190 Beijing, P. R. China. E-mail: zhangli@iccas.ac.cn, liumh@iccas.ac.cn

<sup>b</sup>University of Chinese Academy of Sciences, Beijing 100049, China

<sup>c</sup>CAS Center for Excellence in Nanoscience, CAS Key Laboratory of Nanosystem and Hierarchical Fabrication, Division of Nanophotonics, National Center for Nanoscience and Technology (NCNST), No. 11 ZhongGuanCun BeiYiTiao, Beijing 100190, P. R. China. E-mail: jiangj@nanoctr.cn

† Electronic supplementary information (ESI) available. See DOI: <https://doi.org/10.1039/d4nr04175e>

$F^-$  and amino groups in these units.<sup>46</sup> Secondly, the triarylamine moiety is known to exhibit photochromism due to the formation of a persistent radical anion upon photo-irradiation.<sup>47–49</sup> Notably, upon addition of  $F^-$ , the assembly of the triarylamine derivative **R/S-UNTA** was found to exhibit supramolecular chiral information amplification (Fig. 1). By adjusting the proportion of fluoride ions, it was observed that the CD intensity gradually increased, and the  $g_{\text{abs}}$  value increased by fifteen times. The chiroptical response was described using the absorption dissymmetry factor  $g_{\text{abs}}$  ( $g_{\text{abs}} = (A_L - A_R)/(A_L + A_R)/2$ ), in which  $A_L$  and  $A_R$  represent the absorption of left-handed and right-handed circularly polarized light.<sup>50,51</sup> In addition, **R/S-UNTA** self-assembled to form nano-fibres, and chiral twist nanostructures could be observed in the presence of  $F^-$ , which also corresponds to the obvious enhancement of chiroptical signals.

Moreover, under irradiation with 365 nm ultraviolet light, the assembly of **R/S-UNTA** changed the colour from colourless to dark green, while it quickly changed to red only in the presence of  $F^-$ . The specific chiroptical signal amplification and photochromic effect suggest potential application in sensing  $F^-$ . In contrast, the other chiral triarylamine derivatives containing the amide moiety could not exhibit chiral regulation by  $F^-$  and the corresponding photochromism, implying that the  $-NH$  fragment of the urea subunit establishes the strongest H-bond interaction with  $F^-$ .

## Experimental

### Materials

All reagents and solvents were used as received without further purification. 4,4',4''-Triaminotriphenylamine (98%) was purchased from Ark. (*S*)-(+)-1-(1-Naphthyl) ethyl isocyanate (95%) and

(*R*)-(-)-1-(1-naphthyl) ethyl isocyanate (95%) were purchased from TCI. Triethylamine (AR), tetrabutylammonium fluoride (95%), tetrabutylammonium chloride (95%), and tetrabutylammonium bromide (99%) were purchased from J&K. Tetrabutylammonium nitrate, and tetrabutylammonium methane sulfonate were purchased from Innochem. d2-Dichloromethane and methyl sulphoxide-D6 were purchased from J&K. *N,N*-Dimethylformamide (DMF, AR) and dichloromethane (DCM, AR) were obtained from Beijing Chemical Works, and the water used in all experiments was of Millipore Milli-Q grade (18.2 M $\Omega$  cm).

**S/R-UNTA** and **S/R-ANTA** were synthesized in previous work.<sup>52</sup>

### Preparation of **R/S-UNTA** assemblies with anions

A typical procedure for assembly formation in a DMF : DCM = 2 : 8 solution mixture is as follows: 4.4 mg of **R/S-UNTA** molecules were dispersed in 1 mL DMF and heated to form a transparent solution which was then cooled to 25 °C. After 10 minutes, **R/S-UNTA** solution of fixed concentration was obtained. A DMF solution of **R/S-UNTA** was prepared at the calculated ratio. A poor solvent (DCM) was added to the aforementioned solvent, and the assembly of **R/S-UNTA** was obtained after 30 minutes. The preparation method for the assembly with anionic co-assembly is similar to the aforementioned method. Importantly, the anion's salt is first dissolved in DCM at room temperature and then co-assembled with **R/S-UNTA** according to the calculated ratio.

### Measurements

UV-Vis spectra were recorded using quartz cuvettes (light path 0.1 mm) on a SHIMADZU UV-2600 spectrometer. All the

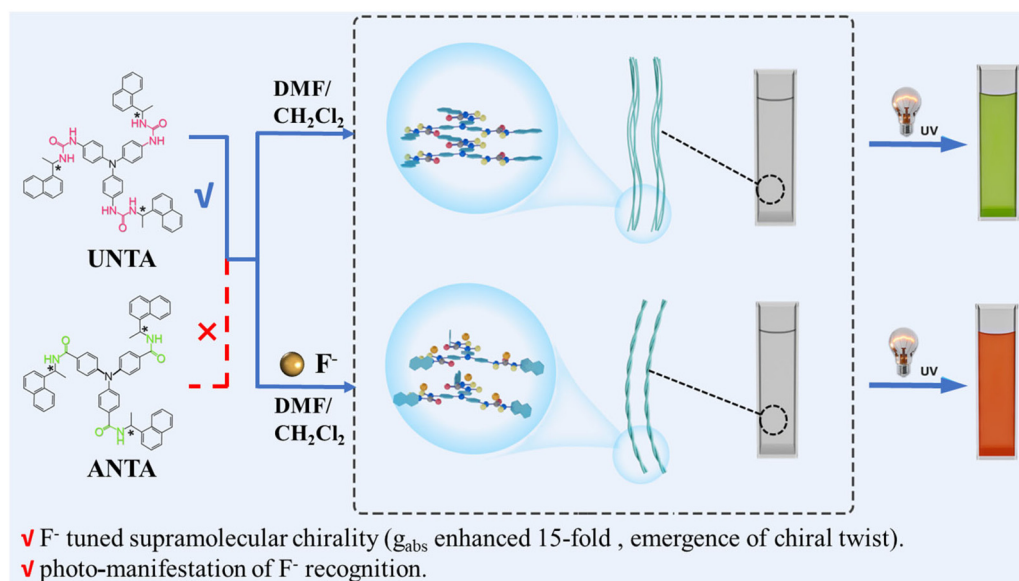


**Fig. 1** Molecular structure of chiral triarylamine derivatives **UNTA** and **ANTA**. **R/S-UNTA** is capable of self-assembling into nanofiber structures when dissolved in a mixed solvent of DMF : DCM = 2 : 8. The co-assembly of **R-UNTA** with  $F^-$  leads to the formation of chiral twist nanostructures. Upon ultraviolet irradiation, the co-assembly containing  $F^-$  displays a colour change that is markedly different from that of the **R-UNTA** self-assembly.

samples were prepared by directly taking the assembly from the test vial. CD spectra were recorded using a cuvette (light path of 0.1 mm) on a JASCO J-1500 spectrophotometer. SEM images were recorded on a Hitachi S-8220 FE-SEM instrument with an accelerating voltage of 10 kV. Samples were cast onto single-crystal silica plates, and the solvent was evaporated under vacuum-dried conditions. The sample surface was coated with a thin layer of Pt to increase the contrast. XRD analysis was performed on a Rigaku D/Max-2500 X-ray diffractometer (Japan) with Cu K $\alpha$  radiation ( $\lambda = 1.5406 \text{ \AA}$ ), which was operated at a voltage of 40 kV and a current of 150 mA. Samples were cast onto larger single-crystal silica plates, and the solvent was evaporated under vacuum-dried conditions for XRD measurements.  $^1\text{H}$  NMR spectra were recorded on a Bruker Advance 400 spectrometer (400 MHz), and the sample was dissolved in a  $d_6$ -dimethyl sulfoxide and  $d_2$ -dichloromethane mixed solvent.

## Results and discussion

### Assembly and chiral properties of *R/S*-UNTA

*R/S*-UNTA and *R/S*-ANTA were synthesized, featuring a triarylamine core connected to chiral naphthalene through urea or amide bonds. Furthermore, the impact of inorganic anions on self-assembly systems based on triarylamine derivatives was investigated. Notably, it was discovered that the introduction of fluoride ions into these systems allows for specific control over the chiral expression. Fig. 2a shows the UV-Vis spectra of *R*-UNTA and its co-assembly with  $\text{F}^-$ . It was observed that the

main peak at 316 nm together with two shoulders at 294 and 284 nm were present when the concentration of *R*-UNTA was  $1 \times 10^{-5} \text{ mol L}^{-1}$  at DMF : DCM = 2 : 8 solvent (grey dashed line), which could be assigned to the  $\pi$ - $\pi^*$  transition of triarylamine. Upon increasing the *R*-UNTA concentration to  $1 \times 10^{-3} \text{ mol L}^{-1}$  within the system (red dashed line), it was found that the absorption peak at 316 nm blue-shifted to 312 nm (Fig. 2a), suggesting that *R*-UNTA was prone to undergo *H*-aggregation. Furthermore, the incorporation of  $\text{F}^-$  into the aforementioned system for co-assembly with *R*-UNTA was investigated. Upon analysis, it was apparent that at a *R*-UNTA concentration of  $1 \times 10^{-5} \text{ mol L}^{-1}$  (depicted by the grey solid line), the introduction of  $\text{F}^-$  had no discernible impact on the UV absorption spectrum of the system. Conversely, when the *R*-UNTA concentration was increased to  $1 \times 10^{-3} \text{ mol L}^{-1}$ , a notable blue shift from 312 nm to 308 nm in the UV absorption peak was observed (depicted by the red solid line), which signifies the co-assembly of  $\text{F}^-$  with *R*-UNTA molecules within the system. This finding underscores the capacity of  $\text{F}^-$  to stimulate further assembly of *R*-UNTA molecules, leading to the formation of a more organized and structured assembly. It is noteworthy that upon co-assembly of  $1 \times 10^{-3} \text{ mol L}^{-1}$  *R*-UNTA with  $\text{F}^-$ , a distinct shoulder peak emerges within the 350–400 nm range. This spectral feature is likely indicative of the absorption peak associated with the formation of dimers, which may be facilitated by the introduction of  $\text{F}^-$ , promoting the assembly of *R*-UNTA molecules.

The chiroptical properties of *R/S*-UNTA were further studied, as shown in Fig. 2b. In the solvent mixture (DMF : DCM = 2 : 8), *R*-UNTA exhibits a weak positive signal at around 315 nm, which is consistent with the absorption band. *S*-UNTA shows a mirror image of *R*-UNTA, with a weak negative Cotton effect observed, suggesting the chiral transfer from chiral carbon to the triarylamine chromophore. Upon introduction of  $\text{F}^-$  into this system, a marked amplification of CD intensity for *R/S*-UNTA is observed (Fig. 2b). To establish the optimal ratio that enhances chiral expression,  $\text{F}^-$  titration experiments were performed using a constant concentration of *R/S*-UNTA. As depicted in Fig. 2c, varying amounts of  $\text{F}^-$  were added to a  $1 \times 10^{-3} \text{ mol L}^{-1}$  *R*-UNTA solution, and their CD spectra were subsequently analysed. Further analysis of the  $g_{\text{abs}}$  in mixed systems containing varying  $\text{F}^-$  concentrations revealed a gradual increase in the  $g_{\text{abs}}$  of *R*-UNTA at 310 nm with the increase of  $\text{F}^-$  content (Fig. 2d and Table S1 $\dagger$ ). And a plateau was observed at 3 : 1, indicating that three equivalents of  $\text{F}^-$  are required to fully elicit the chiral properties of *R/S*-UNTA molecules. Based on the molecular structure of *R/S*-UNTA, it can be hypothesized that  $\text{F}^-$  interacts with the urea bond, fostering multi-level assembly and enhancing chiral expression. However, at a concentration of  $1 \times 10^{-5} \text{ mol L}^{-1}$ , *R/S*-UNTA exists predominantly in a single-molecule state within the mixed solvent (DMF : DCM = 2 : 8). The introduction of  $\text{F}^-$  into this system fails to elicit a substantial increase in the CD signal, as depicted in Fig. S1 $\dagger$ . This observation underscores the necessity for the *R/S*-UNTA concentration to surpass a certain threshold, enabling the formation of assemblies, before

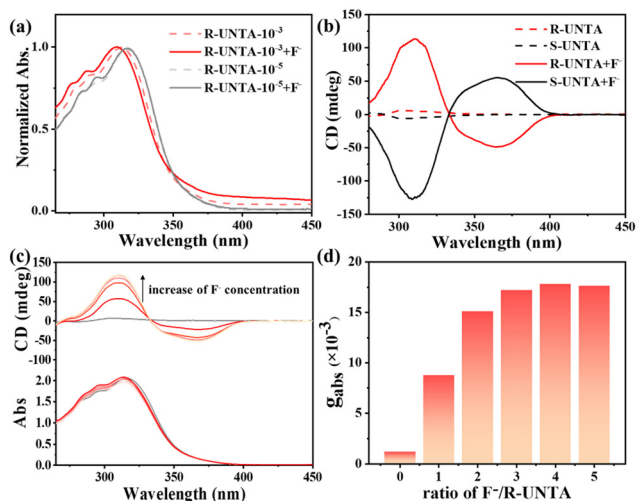


**Fig. 2** (a) Absorption spectra of different concentrations of *R*-UNTA and the *R*-UNTA co-assembly with  $\text{F}^-$  in DMF : DCM = 2 : 8. (b) CD spectra of *R*-UNTA (red dashed line), *S*-UNTA (black dashed line), and the *R*-UNTA co-assembly with  $\text{F}^-$  (red solid line), *S*-UNTA with  $\text{F}^-$  (black solid line) (concentrations of UNTA and  $\text{F}^-$  are  $1 \times 10^{-3} \text{ mol L}^{-1}$  and  $3 \times 10^{-3} \text{ mol L}^{-1}$ , respectively, the solvent is DMF : DCM = 2 : 8). (c) CD spectra of *R*-UNTA solution upon adding varying amounts of  $\text{F}^-$ . (d) The different concentrations of  $\text{F}^-$  result in alterations in the  $g_{\text{abs}}$  values of the samples (concentration of *R*-UNTA is  $1 \times 10^{-3} \text{ mol L}^{-1}$ ).

the CD signal can be significantly modulated by the presence of  $F^-$ . We also detected other kinds of anions, such as  $Cl^-$ ,  $Br^-$ ,  $NO_3^-$ , and  $CH_3SO_3^-$ , and it was shown that the CD signal could not be enhanced by the addition of other anions, as shown in Fig. S2,† which implied the specific selectivity to  $F^-$ .

To elucidate the pivotal role of the urea bond in the chiral manifestation of  $F^-$  on the molecular structure of the chiral triarylamine derivative *R/S*-UNTA, we strategically designed and synthesized a molecular analogue, *R/S*-ANTA, featuring a similar molecular backbone but with the urea bond substituted by an amide bond. Subsequently, CD spectroscopic analyses were conducted on self-assembled samples of *R/S*-ANTA, as well as on co-assembled samples of  $F^-$  and *R/S*-ANTA. As evident in Fig. S3,† the *R*-ANTA enantiomer displays a pronounced positive CD signal within the 250 nm–350 nm range, and the introduction of  $F^-$  does not appreciably amplify this signal. Analogously, *S*-ANTA exhibits a negative CD signal in the same spectral region, with no discernible alteration upon  $F^-$  addition. This comparative investigation underscores the unique interaction between urea and  $F^-$ , which significantly augments the chiral expression in *R/S*-UNTA, thereby validating the hypothesis regarding the urea bond's decisive function.

### Chiral twists of *R/S*-UNTA induced by $F^-$

Based on the experimental data analysis presented, the co-assembly of *R/S*-UNTA and  $F^-$  markedly amplifies the chiral signal expression. This enhancement is evident in the CD absorption spectrum, where the  $g_{abs}$  value increases by over an order of magnitude. To further elucidate the underlying microstructural changes, scanning electron microscopy (SEM) was employed to assess the chiral expression. As depicted in Fig. 3a, individual *R*-UNTA molecules assembled in the mixed solvent form a nanofiber network with entanglements but lack a discernible chiral structure, correlating with relatively weak CD signals.

In contrast, the co-assembly of  $F^-$  with *R*-UNTA in the same solvent mixture (DMF : DCM = 2 : 8) exhibits a distinct chiral nanostructure (Fig. 3b and S4†). SEM characterization reveals the formation of numerous entangled chiral twists, indicating that  $F^-$  interacts with *R*-UNTA and enhances chiral accumulation of molecular chirality in UNTA, corresponding to the highest CD signal intensity. We conducted extensive SEM morphology analysis and observed that structural chirality positively correlated with molecular chirality in all images. Furthermore, during the sample characterization process, we did not observe the simultaneous appearance of left-handed and right-handed helical structures in the same sample. The co-assembly of *S*-UNTA with  $F^-$  in mixed solvents has been investigated, revealing a morphology that is the mirror image of the *R*-UNTA chiral structure. Notably, while *R*-UNTA assemblies exhibit a right-handed helical sense, the *S*-UNTA assemblies display a complementary left-handed helicity (Fig. 3c). We have acquired SEM images of samples with low  $F^-$  concentration, as presented in Fig. S5.† These images reveal that under the conditions of low  $F^-$  concentration, the concentration of  $F^-$  does not exceed the critical threshold required for promoting the multi-stage assembly of *R/S*-UNTA molecules. As a result, the microstructure during the co-assembly process is found to be consistent with that observed during the self-assembly of *R/S*-UNTA molecules.

Particle size analysis of the samples (Fig. 3d, f, e and S6†) reveals that the *R*-UNTA self-assembly in the mixed solvent (DMF : DCM = 2 : 8) yields nanofiber structures with a width around 67.36 nm, whereas the co-assembly of  $F^-$  and *R/S*-UNTA results in structures with a larger size, with widths of about 112.79 nm (*R*-UNTA) and 122.44 nm (*S*-UNTA). Additionally, the morphological changes following the co-assembly of *R*-UNTA with varying equivalents of  $F^-$  were investigated, as depicted in Fig. S7a.† When one equivalent of  $F^-$

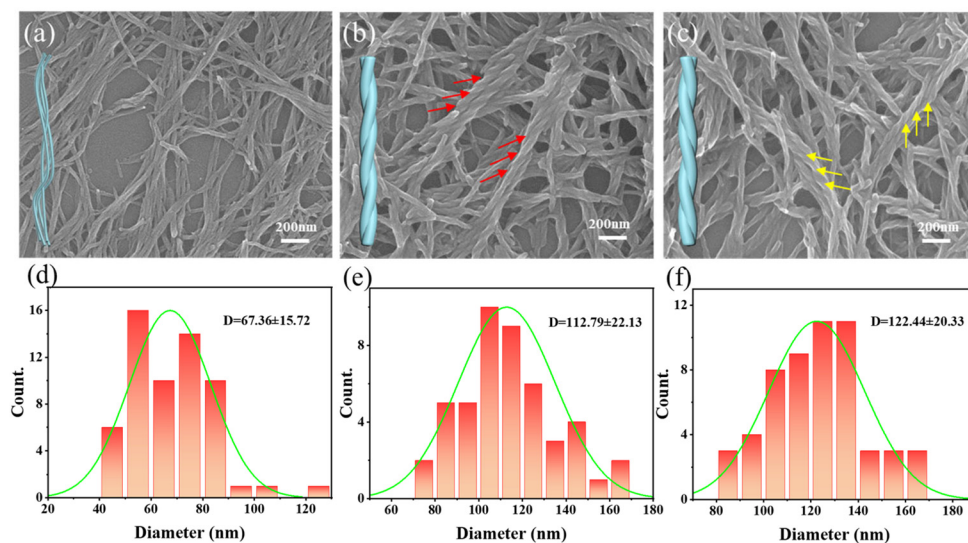


**Fig. 3** SEM images of the (a) *R*-UNTA self-assembly, (b) *R*-UNTA/ $F^-$  co-assembly, and (c) *S*-UNTA/ $F^-$  co-assembly; and particle size analysis of the (d) *R*-UNTA self-assembly, (e) *R*-UNTA/ $F^-$  co-assembly and (f) *S*-UNTA/ $F^-$  co-assembly (solvent ratio is DMF : DCM = 2 : 8).

was co-assembled with *R*-UNTA, a multitude of short rod-shaped structures were distinctly observed in the SEM image. This observation suggests that a small quantity of F<sup>-</sup> co-assembled with *R*-UNTA can enhance the rigidity of the assembly structure. However, due to the low concentration of F<sup>-</sup>, the co-assembly does not result in the formation of a long-range ordered structure. As the concentration of F<sup>-</sup> increases, as illustrated in Fig. S7b–d,† a regular twist structure begins to emerge in the SEM image. SEM analysis also indirectly confirms that three equivalents of F<sup>-</sup> co-assembled with *R*-UNTA, enabling full expression of its chirality.

### Characterization of the assembly structure based on *R/S*-UNTA

To delve deeper into the assembly mechanism underlying the interaction between F<sup>-</sup> and *R*-UNTA, we conducted comprehensive structural analyses on both self-assembled *R*-UNTA samples and co-assembled F<sup>-</sup>/*R*-UNTA samples in a mixed solvent (DMF:DCM = 2:8). As depicted in Fig. 4a, the <sup>1</sup>H nuclear magnetic resonance (NMR) spectrum reveals distinct N–H vibrational peaks at  $\delta = 8.27$  ppm (H<sub>a</sub>) and  $\delta = 6.66$  ppm (H<sub>b</sub>) within the *R*-UNTA molecular structure. Upon performing nuclear magnetic titration with increasing F<sup>-</sup> content, these peaks underwent a pronounced shift towards lower fields, ultimately diminishing and disappearing, indicative of F<sup>-</sup> interaction with urea bonds, disrupting the intramolecular hydrogen bonding network in *R*-UNTA. This suggests that F<sup>-</sup> acts as a bridge between two *R*-UNTA molecules, constraining the naphthalene headgroup's rotational freedom, enhancing the rigidity of the *R*-UNTA assembly, and facilitating chirality transfer from chiral carbon centres to chiral nano-helical structures.

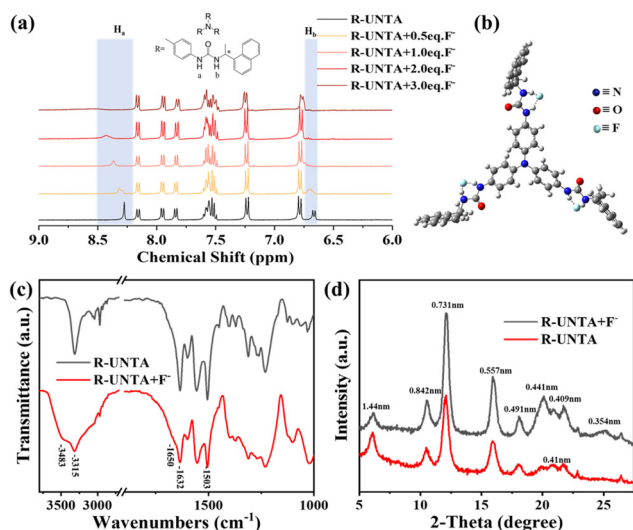


**Fig. 4** (a) <sup>1</sup>H NMR spectra of *R*-UNTA at different equivalents of F<sup>-</sup> (DMF : DCM = 2 : 8). (b) The snapshot of the *R*-UNTA/F<sup>-</sup> co-assembly in a mixed solvent (DMF : DCM = 2 : 8). (c) FT-IR spectra of *R*-UNTA and the *R*-UNTA/F<sup>-</sup> co-assembly. (d) XRD pattern of *R*-UNTA and the *R*-UNTA/F<sup>-</sup> co-assembly.

Additionally, FT-IR spectroscopy of *R*-UNTA assemblies displays strong vibrational peaks at 3315, 1632, and 1503 cm<sup>-1</sup>, indicative of the N–H stretching vibration band of urea, the C=O stretching vibration band, and the N–H bending vibration band, respectively (Fig. 4c). Upon addition of F<sup>-</sup>, a shoulder peak emerged at 3483 cm<sup>-1</sup>, accompanied by a shoulder peak at 1650 cm<sup>-1</sup>, reflecting the hydrogen bonding in the urea moiety, probably affected by the presence of F<sup>-</sup>. The coordination of F<sup>-</sup> with the N–H group on the urea bond results in the liberation of the carbonyl and amine groups, which may cause the appearance of shoulder bands at 3483 and 1650 cm<sup>-1</sup>. Furthermore, XRD analysis (Fig. 4d) of both *R*-UNTA and *R*-UNTA/F<sup>-</sup> co-assemblies revealed a hexagonal stacking pattern, with characteristic interlayer spacings corresponding to a ratio close to 1 : 1/√3 : 1/√4 : 1/√7 : 1/√9, confirming the formation of a well-ordered structure. The co-assembled *R*-UNTA/F<sup>-</sup> sample exhibited more sophisticated π–π stacking, which was indicative of peaks at 0.41 nm and 0.44 nm.

Based on the analysis of the aforementioned results, a plausible mechanism is proposed for how the co-assembly of F<sup>-</sup> with *R/S*-UNTA facilitates the formation of helical assemblies through coordination interactions between the *R*-UNTA molecules and F<sup>-</sup>, as illustrated in Fig. 5. Tetra-*n*-butylammonium fluoride molecules are present in their ionic form in DMF : DCM = 2 : 8, and it is in this form that F<sup>-</sup> coordinates with chiral *R/S*-UNTA to form assemblies. The introduction of F<sup>-</sup> *R*-UNTA results in a significant change in the molecular conformation. Post-Gaussian simulation analysis reveals that the dihedral angle between the naphthalene and the central triarylamine moiety increases from approximately 30° to around 90°. Concurrently, the nitrogen atom adjacent to the naphthalene in the N–H group transitions from sp<sup>2</sup> to sp<sup>3</sup> hybridization. Consequently, the molecular asymmetry is enhanced, and as two molecules approach each other to form assemblies, the central triarylamine framework is brought

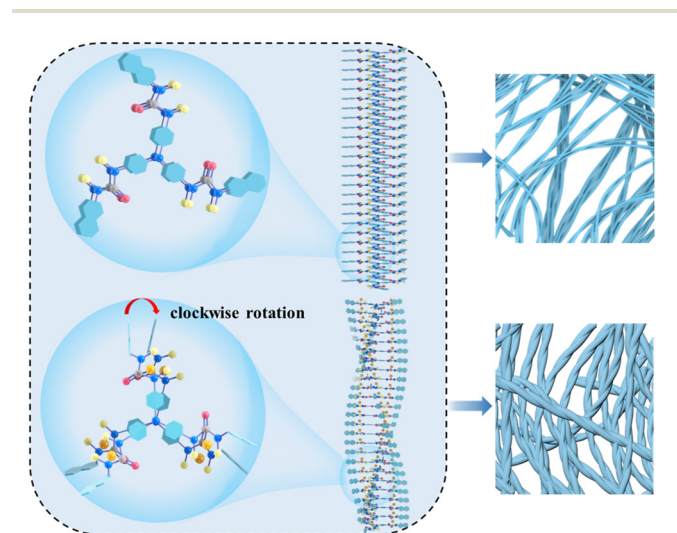


**Fig. 5** Illustration of the mechanism of F<sup>-</sup>-induced chirality control of *R*-UNTA.

closer by  $\pi$ - $\pi$  interactions. Meanwhile, the bulky nature of the peripheral naphthalene rings increases steric hindrance, forcing the molecules to adopt a dislocated stacking arrangement. This leads to the continuous accumulation and amplification of molecular chirality within the dislocation stacking, manifesting as a macroscopic chiral twist morphology. This chiral arrangement allows for the maintenance of intermolecular interactions while minimizing adverse spatial effects to the greatest extent possible.

### Specific selectivity of *R/S*-UNTA for fluoride ions

The specific selectivity of *R/S*-UNTA towards  $F^-$  represents a notable feature of its chemical behaviour. This selectivity underscores the capacity of *R/S*-UNTA to discern and preferentially interact with fluoride ions, highlighting its potential applications in fields requiring targeted recognition and manipulation of fluoride species.<sup>53</sup>

Triaryl amines exhibit a low ionization potential owing to the conjugation of nitrogen electron pairs with benzene rings, a property that predisposes TPA derivatives to generate TPA radical cations under oxidative and photolytic conditions, thereby attracting our research interest. Then, we explored the photoresponsiveness of the *R/S*-UNTA system in the presence of various anions. Upon subjecting the aforementioned system to ultraviolet light irradiation, a notable difference in colorimetric response was observed between the co-assembly system containing  $F^-$  and the *R*-UNTA self-assembly system. Specifically, while irradiation of *R*-UNTA alone in a mixed solvent of DMF and DCM results in the gradual emergence of an emerald green color, the introduction of  $F^-$  leads to a distinctive red coloration upon UV exposure. This observation indicates that the specific recognition of  $F^-$  can be manifested by photoirradiation.

To probe the selectivity of *R*-UNTA towards  $F^-$ , we performed a comparative study by co-assembling *R*-UNTA with various inorganic anions ( $F^-$ ,  $Cl^-$ ,  $Br^-$ ,  $NO_3^-$ ,  $CH_3SO_3^-$ ). As shown in Fig. 6a, the resulting solutions were initially colourless and transparent. Upon irradiation with 365 nm UV light for 10 minutes, a marked visual differentiation emerged: the system containing  $F^-$  displayed a pronounced red colour, whereas systems incorporating other anions exhibited a greenish colour. This clearly demonstrates the specific selectivity of *R*-UNTA towards  $F^-$ , manifested as a macroscopic colour change observable by the naked eye.

Further analysis *via* UV-Vis absorption spectroscopy (Fig. 6b and c) corroborated these findings. Prior to UV irradiation, the co-assembled systems containing various anions exhibited UV absorption profiles akin to that of the *R*-UNTA self-assembly. However, upon irradiation with 365 nm UV light, only the system with  $F^-$  displayed a pronounced absorption peak at 500 nm, which was ascribed to the appearance of a charge-transfer absorption band in the visible region. Distinction from the peaks emerged at around 420 nm was observed for the *R*-UNTA self-assembly and co-assemblies with other anions, respectively. This spectral profile is constant with a drastic colour change under UV irradiation.

The investigation focused on the changes in UV absorption spectra of *R*-UNTA/ $F^-$  co-assemblies following UV irradiation, as

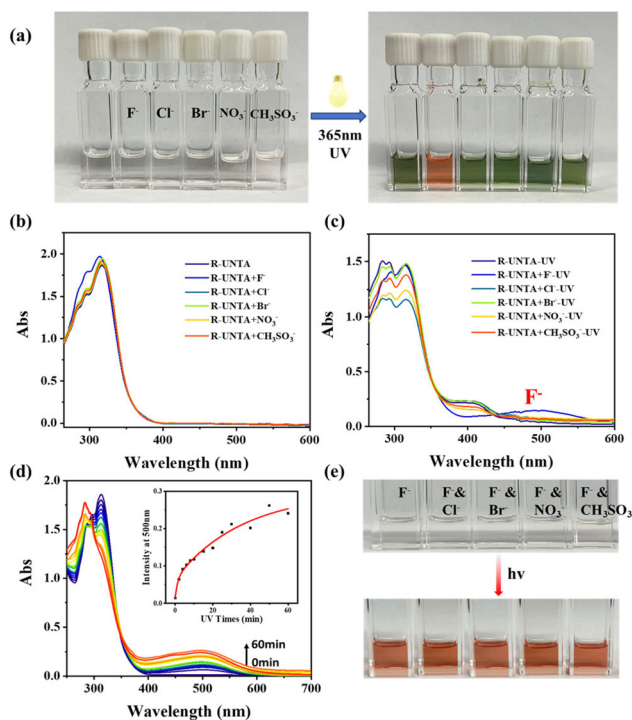


**Fig. 6** (a) Colorimetric response of *R*-UNTA upon the addition of different anions. (b) Absorption spectra of *R*-UNTA upon the addition of different anions. (c) Absorption spectra of *R*-UNTA after adding different anions and irradiating with 365 nm ultraviolet light for 10 minutes (DMF : DCM = 2 : 8). (d) Absorption spectra of the *R*-UNTA co-assembly with  $F^-$  upon irradiation with 365 nm UV light for 60 minutes. (e) Colorimetric response of *R*-UNTA upon the addition of 3 eq. of  $F^-$  and 3 eq. of different anions ( $F^-$ ,  $Cl^-$ ,  $Br^-$ ,  $NO_3^-$ , and  $CH_3SO_3^-$ ).

depicted in Fig. 6d. Consistent with the above findings, a new broad absorption peak emerged at 500 nm in the system, and the intensity of this peak gradually increased with the extension of the UV irradiation period. The absorption intensity at 500 nm initially increased rapidly, and after a certain duration of irradiation, the rate of increase slowed down, eventually stabilizing at around 20 min. This analysis suggests that the *R*-UNTA/ $F^-$  co-assembly exhibits heightened sensitivity to UV irradiation, capable of generating a notably strong absorption peak at 500 nm within a short irradiation timeframe. Macroscopically, the system can undergo a colour change in a very short period through UV irradiation, indicating a rapid response to the UV light stimulus. Fig. S11† shows the CD spectra of *R*-UNTA after UV irradiation. The CD peak at 310 nm significantly decreases and undergoes a blue shift after UV irradiation, indicating that UV irradiation disrupts the orderliness of the *R*-UNTA/ $F^-$  co-assembly. In comparison, the analogous compound *R*-ANTA did not exhibit photochromism upon photo-irradiation, both with and without the addition of  $F^-$ , indicating that *R*-ANTA is unable to form stable radical ions, which is consistent with our previous reports. (Fig. S12†) Additionally, the introduction of  $F^-$  and other anions does not increase the stability of the radical ions of *R*-ANTA.

To deepen our understanding of the impact of ultraviolet (UV) irradiation on *R/S*-UNTA, an investigation was conducted

into the morphological changes that occurred after 10 and 30 minutes of exposure. SEM analysis revealed that upon exposure to UV light for a defined period, the microstructure of **R-UNTA** evolved into a network composed of an extensive array of intertwined short fibres (Fig. S13 and S14†). In contrast, the **R-UNTA/F<sup>-</sup>** co-assembly exhibited a structure characterized by a multitude of rigid, rod-shaped fibre shuttles. These observations suggest that UV irradiation conditions are not conducive to the induction of chirality from the molecular to the supramolecular level. The XRD profile showed that upon photoirradiation, the diffraction peak intensities of **R-UNTA/F<sup>-</sup>** decreased in comparison to **R-UNTA**, with a particularly marked reduction observed at the 1.44 nm peak, suggesting a decrease in the structural order (Fig. S15†). This observation is consistent with the less ordered structure revealed in the SEM images.

The mechanism of the colour change resulting from the interaction between F<sup>-</sup> and urea bonds has also been studied in previous works.<sup>34</sup> Under ultraviolet irradiation, triarylamine molecules are excited to high-energy states, which is usually the first step in generating free radical cations. Excited triarylamine molecules have higher reactivity and can participate in subsequent electron transfer processes. In chlorine-containing solvents, the triarylamine molecule TPA generates a free radical TPA<sup>+•</sup> by absorbing photons, and then electrons transfer from the central N to the chlorine adjacent to the chloroform molecule, resulting in the formation of a charge transfer complex (TPA<sup>+•</sup> + Cl<sup>-</sup>), and we confirmed the generation of the TPA radical using EPR and NMR techniques in our previous work.<sup>52</sup> When F<sup>-</sup> was introduced into the irradiated **UNTA** system, it induced deprotonation of the -NH fragment of the urea subunit. Subsequently, a charge-transfer transition from the -NH fragment to the -N<sup>+•</sup> moiety occurred, leading to the appearance of charge transfer absorption bands and drastic colour changes in the visible light region.

Ultimately, the study aimed to assess the anti-interference capability of the **R-UNTA/F<sup>-</sup>** co-assembly in the presence of other ions. To this end, three equivalents of various anions (Cl<sup>-</sup>, Br<sup>-</sup>, NO<sub>3</sub><sup>-</sup>, and CH<sub>3</sub>SO<sub>3</sub><sup>-</sup>) were introduced to the **R-UNTA** assembly already containing F<sup>-</sup>. The colorimetric analysis revealed that the resulting solutions were colourless and transparent (Fig. 6e). Upon exposure to UV irradiation, it was observed that all colorimetric dishes displayed a red coloration. This response is consistent with the photochromism of the individual **R-UNTA/F<sup>-</sup>** co-assembly under the same UV irradiation conditions, thereby indicating that the **R-UNTA/F<sup>-</sup>** co-assembly has a strong tolerance to interference from other anions in the system. Moreover, as shown in Fig. S18,† the addition of F<sup>-</sup> into the UV irradiated solution of **R-UNTA** also caused a drastic colour change from green to reddish.

## Conclusions

Our findings establish the importance of fluoride ions in the regulation of supramolecular chirality in the self-assembly

systems of chiral compounds. We have demonstrated that the introduction of fluoride ions into these systems can selectively amplify supramolecular chirality, as evidenced by the enhancement of CD signals and the emergence of macroscopic chiral twist nanostructures. The specific selectivity of urea for fluoride ions in the **R/S-UNTA** system, as confirmed by comparative studies with various other anions, underscores its potential utility as a chiroptical sensor with selectivity for fluoride detection. Moreover, by utilizing the photoproduct triarylamine radical anions, F<sup>-</sup> could be identified by the distinct colour change upon photo-irradiation. This study provides an avenue for the development of stimuli-responsive chiral supramolecular systems, with exciting prospects for application in the fields of sensing and chiroptical technology.

## Author contributions

J. Jiang, L. Zhang and M.H. Liu conceived the research and led the study. S.J. Ma conducted the majority of experiments and performed analysis of the data. X. Wen synthesized the compounds. S.J. Ma and L. Zhang drafted the manuscript. All authors revised and reviewed the manuscript.

## Data availability

All data are provided in the manuscript and the ESI.†

## Conflicts of interest

There are no conflicts to declare.

## Acknowledgements

We gratefully acknowledge financial support from the National Natural Science Foundation of China (92356302 and 92156018), the National Key R&D Program of China (2021YFA1200301), and the CAS Project for Young Scientists in Basic Research (YSBR-027).

## References

- 1 M. Liu, L. Zhang and T. Wang, *Chem. Rev.*, 2015, **115**, 7304–7397.
- 2 L. Zhang, M. Deng, Y. Duan, X. Wen, Y. Jiang, H. Jiang, Y. Ma and M. Liu, *Nano Res.*, 2021, **15**, 1079–1086.
- 3 S. Datta, Y. Kato, S. Higashiharaguchi, K. Aratsu, A. Isobe, T. Saito, D. D. Prabhu, Y. Kitamoto, M. J. Hollamby, A. J. Smith, R. Dalgliesh, N. Mahmoudi, L. Pesce, C. Perego, G. M. Pavan and S. Yagai, *Nature*, 2020, **583**, 400–405.
- 4 C. Du, Z. Li, X. Zhu, G. Ouyang and M. Liu, *Nat. Nanotechnol.*, 2022, **17**, 1294–1302.

- 5 S. Du, Y. Jiang, H. Jiang, L. Zhang and M. Liu, *Angew. Chem., Int. Ed.*, 2024, **63**, e202316863.
- 6 T. Mori, *Angew. Chem., Int. Ed.*, 2024, **63**, e202319702.
- 7 J. Kim, J. Lee, W. Y. Kim, H. Kim, S. Lee, H. C. Lee, Y. S. Lee, M. Seo and S. Y. Kim, *Nat. Commun.*, 2015, **6**, 7959.
- 8 F. Zhang, F. Yang, Y. Gong, Y. Wei, Y. Yang, J. Wei, Z. Yang and M. P. Pileni, *Small*, 2020, **16**, 2005701.
- 9 S. Ma, J. Jiang, Z. Liu, Y. Jiang, Z. Wu and M. Liu, *Nanoscale*, 2020, **12**, 7895–7901.
- 10 S. Xie, W. Sun, J. Sun, X. Wan and J. Zhang, *Nat. Commun.*, 2023, **14**, 6496.
- 11 X. Dou, N. Mehwish, C. Zhao, J. Liu, C. Xing and C. Feng, *Acc. Chem. Res.*, 2020, **53**, 852–862.
- 12 K. Qi, H. Qi, M. Wang, X. Ma, Y. Wang, Q. Yao, W. Liu, Y. Zhao, J. Wang, Y. Wang, W. Qi, J. Zhang, J. R. Lu and H. Xu, *Nat. Commun.*, 2024, **15**, 6186.
- 13 J. Liu, F. Yuan, X. Ma, D. i. Y. Auphedeous, C. Zhao, C. Liu, C. Shen and C. Feng, *Angew. Chem., Int. Ed.*, 2018, **57**, 6475–6479.
- 14 D. Niu, L. Ji, G. Ouyang and M. Liu, *ACS Appl. Mater. Interfaces*, 2020, **12**, 18148–18156.
- 15 S. Du, Y. Wang, F. Wang, T. Wang, L. Zhang and M. Liu, *Chin. Chem. Lett.*, 2024, **35**, 109256.
- 16 H. Ma, X. Cheng, G. Zhang, T. Miao, Z. He and W. Zhang, *Adv. Sci.*, 2024, **11**, 2308371.
- 17 Q. Zhang, A. Hao and P. Xing, *ACS Nano*, 2023, **17**, 9468–9477.
- 18 W. Kang, Y. Tang, X. Meng, S. Lin, X. Zhang, J. Guo and Q. Li, *Angew. Chem., Int. Ed.*, 2023, **62**, e202311486.
- 19 H. Jiang, Y. Jiang, J. Han, L. Zhang and M. Liu, *Angew. Chem., Int. Ed.*, 2018, **58**, 785–790.
- 20 S. Lin, T. Ren, X. Meng, W. Kang and J. Guo, *Sci. China: Chem.*, 2024, **67**, 2719–2727.
- 21 Z. Huang, Z. He, B. Ding, H. Tian and X. Ma, *Nat. Commun.*, 2022, **13**, 7841.
- 22 K. Yao, Z. Liu, H. Li, D. Xu, W.-H. Zheng, Y.-W. Quan and Y.-X. Cheng, *Sci. China: Chem.*, 2022, **65**, 1945–1952.
- 23 S. Takahashi and S. Yagai, *J. Am. Chem. Soc.*, 2022, **144**, 13374–13383.
- 24 Q. He, D. H. Tuo, Y. F. Ao, Q. Q. Wang and D. X. Wang, *ACS Appl. Mater. Interfaces*, 2018, **10**, 3181–3185.
- 25 Q. Cheng, A. Hao and P. Xing, *Nat. Commun.*, 2021, **12**, 6320.
- 26 N. Busschaert, C. Caltagirone, W. Van Rossom and P. A. Gale, *Chem. Rev.*, 2015, **115**, 8038–8155.
- 27 P. D. Beer, A. Arun and A. Docker, *Chem. – Eur. J.*, 2024, e202402731, DOI: [10.1002/chem.202402731](https://doi.org/10.1002/chem.202402731).
- 28 G. Picci, R. Montis, A. M. Gilchrist, P. A. Gale and C. Caltagirone, *Coord. Chem. Rev.*, 2024, **501**, 215561.
- 29 Y. Qiu, Y. Zhang, Q. Jiang, H. Wang, Y. Liao, H. Zhou and X. Xie, *Macromolecules*, 2022, **55**, 9057–9065.
- 30 G. Li, Y. Wang, L. Wang, A. Song and J. Hao, *Langmuir*, 2016, **32**, 12100–12109.
- 31 Y. Liu, A. Hao and P. Xing, *Chem. Sci.*, 2024, **15**, 15790–15798.
- 32 M. Zeng, X. Chen and J. Zhang, *Chem. – Eur. J.*, 2023, **29**, e202301827.
- 33 P. A. Gale and C. Caltagirone, *Chem. Soc. Rev.*, 2015, **44**, 4212–4227.
- 34 M. Boiocchi, L. Del Boca, D. E. Gómez, L. Fabbri, M. Licchelli and E. Monzani, *J. Am. Chem. Soc.*, 2004, **126**, 16507–16514.
- 35 H. S. Horowitz, *J. Public Health Dent*, 2007, **63**, 3–8.
- 36 M. Kleerekoper, *Endocrinol. Metab. Clin. North Am.*, 1998, **27**, 441–452.
- 37 M. A. Kerdoun, S. Mekhloufi, O. E. K. Adjaine, Z. Bechki, M. Gana and H. Belkhalifa, *Regul. Toxicol. Pharmacol.*, 2022, **128**, 105086.
- 38 E. Heilbronn, M. Johansson, L. M. Jackman and D. R. Sparrow, *Acta Chem. Scand.*, 1964, **18**, 2410.
- 39 I. A. Revelo-Mejía, R. Gutiérrez-Idrobo, V. A. López-Fernández, A. López-Rosales, F. C. Astaiza-Montenegro, L. Garcés-Rengifo, P. A. López-Ordoñez, A. Hardisson, C. Rubio, Á. J. Gutiérrez and S. Paz, *Environ. Monit. Assess.*, 2022, **194**, 327.
- 40 Q. He, P. Tu and J. L. Sessler, *Chem*, 2018, **4**, 46–93.
- 41 D. V. Vishnevetskii, Y. V. Andrianova, E. E. Polyakova, A. I. Ivanova and A. R. Mekhtiev, *Gels*, 2024, **10**, 332–346.
- 42 W. Chen, X. Tang, W. Dou, B. Wang, L. Guo, Z. Ju and W. Liu, *Chem. – Eur. J.*, 2017, **23**, 9804–9811.
- 43 M. Mulvee, N. Vasiljevic, S. Mann and A. J. Patil, *Gels*, 2021, **7**, 146–161.
- 44 M. Yu, C. Zhao, K. Feng, B. Chen, C. Tung, Y. S. Zheng and L. Wu, *Chin. J. Chem.*, 2011, **29**, 2684–2688.
- 45 E. J. Cho, B. J. Ryu, Y. J. Lee and K. C. Nam, *Org. Lett.*, 2005, **7**, 2607–2609.
- 46 L. Pfeifer, K. M. Engle, G. W. Pidgeon, H. A. Sparkes, A. L. Thompson, J. M. Brown and V. Gouverneur, *J. Am. Chem. Soc.*, 2016, **138**, 13314–13325.
- 47 G. Huo, X. Shi, Q. Tu, Y. Hu, G. Wu, G. Yin, X. Li, L. Xu, H. Ding and H. Yang, *J. Am. Chem. Soc.*, 2019, **141**, 16014–16023.
- 48 Y. Mu, Y. Liu, H. Tian, D. Ou, L. Gong, J. Zhao, Y. Zhang, Y. Huo, Z. Yang and Z. Chi, *Angew. Chem., Int. Ed.*, 2021, **60**, 6367–6371.
- 49 E. Moulin, F. Niess, M. Maaloum, E. Buhler, I. Nyrkova and N. Giuseppone, *Angew. Chem., Int. Ed.*, 2010, **49**, 6974–6978.
- 50 H. Tanaka, Y. Inoue and T. Mori, *ChemPhotoChem*, 2018, **2**, 386–402.
- 51 T. Mori, *Chem. Rev.*, 2021, **121**, 2373–2412.
- 52 B. J. Zhang, C. Du, X. Wen, L. Zhang, R. Duan and M. H. Liu, *Small Methods*, 2024, DOI: [10.1002/smt.202400538](https://doi.org/10.1002/smt.202400538).
- 53 M. Cametti and K. Rissanen, *Chem. Soc. Rev.*, 2013, **42**, 2016–2038.